

Entanglement and its relationship to classical dynamics

Joshua B. Ruebeck, Jie Lin, and Arjendu K. Pattanayak

Department of Physics and Astronomy, Carleton College, Northfield, Minnesota 55057, USA

(Received 15 July 2016; revised manuscript received 1 April 2017; published 26 June 2017)

We present an analysis of the entangling quantum kicked top focusing on the few qubit case and the initial condition dependence of the time-averaged entanglement S_Q for spin-coherent states. We show a very strong connection between the classical phase space and the initial condition dependence of S_Q even for the extreme case of two spin-1/2 qubits. This correlation is not related directly to chaos in the classical dynamics. We introduce a measure of the behavior of a classical trajectory which correlates far better with the entanglement and show that the maps of classical and quantum initial-condition dependence are both organized around the symmetry points of the Hamiltonian. We also show clear (quasi-)periodicity in entanglement as a function of number of kicks and of kick strength.

DOI: [10.1103/PhysRevE.95.062222](https://doi.org/10.1103/PhysRevE.95.062222)

I. INTRODUCTION

The relationship between the entanglement of a nonlinear quantum system and the dynamics of its chaotic classical limit is deeply intriguing since entanglement is quintessentially quantal and chaos quintessentially classical. It has been extensively studied both theoretically and experimentally for over two decades [1–9] and continues to be investigated today [10,11].

One paradigmatic model system is the “kicked top,” consisting of a nonlinearly evolving spin composed of $2j$ qubits and with total spin \vec{J} . The quantum behavior is usually mapped by studying the entanglement dynamics of spin-coherent states initialized at various locations in the phase space. While different measures of the quantum entanglement can be studied, the standard analysis considers the time-dependent entanglement between any one qubit and the other $2j - 1$ qubits. This behavior is then compared with the classical point dynamics of initial conditions corresponding to the locations of the centroids of the spin-coherent states. Studies of this system have considered systems with the quantum number ranging from $j = 8$ up to $j \approx 250$.

The common wisdom about the broad characteristics of the system behavior can be summarized as follows: If a spin-coherent state has an initial centroid location such that the corresponding classical trajectory is chaotic, then (a) the quantum entanglement between the subsystems depends on the classical largest Lyapunov exponent λ (which measures the degree of classical chaos) and moreover follows changes in the behavior of λ with system parameters, and (b) more generally, the asymptotic entanglement and the time-averaged entanglement for these “chaotic” initial states is significantly greater than for states with initial centroids corresponding to regular classical trajectories. Finally, it is understood that (c) this “entanglement as quantum signature of classical chaos” becomes more distinct as the number of spins j increases, that is, as the effective \hbar decreases in the correspondence limit. The reason for this connection is argued broadly as follows: Classically chaotic initial conditions explore phase space more widely. Thus, if a quantum system corresponding to a classically chaotic initial condition similarly explores Hilbert space widely, and given that the generic Hilbert space

state is entangled, the average entanglement is consequently greater for such a quantum system.

Dissenters from this consensus include Lombardi and Matzkin [9] who have argued with specific counterexamples that high quantum entanglement can occur for initial conditions with centroids initialized in classically regular regions. These authors further compare the entanglement with an analogous quantity for a classical probability distribution, deriving from the premise that the classical and quantum (expectation value) dynamics agree with each other for longer times for classical probability distributions than for individual classical initial conditions. Unfortunately, the classical distribution calculations are computationally expensive, prohibiting a full scan of the phase space and a verification of this idea. It is worth noting that all arguments to date have evoked the correspondence principle in explaining the relationship between the classical and quantum behavior. Further, statements about “correlations” between measures have not been quantified and rely on the visual similarity of various figures.

In this paper, we present results from a somewhat different perspective on this issue. We work at small j , corresponding to recent experiments [10] and focusing in particular on two coupled spin-1/2 qubits ($j = 1$). For this system we are able to analytically calculate the infinite-time-averaged quantum entanglement S_Q of initial spin-coherent states. We see that S_Q depends strongly on the initial location of the spin-coherent state. We also see that the geometry emerging from plots of the initial condition dependence of S_Q correlates strongly with the geometry of the classical phase space even for this extreme case where the quantum and classical trajectories disagree immediately and the correspondence principle cannot be evoked. However, high S_Q does not correlate with classical chaos. In particular, we see that classically regular dynamics corresponds to either high or low entanglement, depending on the properties of the orbit, while classically chaotic dynamics correspond to entanglement levels about halfway between these extremes.

In order to better explore and understand this unusual result, we first systematize the so far loose notion of the correlation between the various functions of initial conditions that we use to characterize the systems. That is, the strength

of correlations between various measures is quantified using a generalized Kullback-Liebler distance rather than the usual visual inspection. Second, we introduce a measure I_C of the “ignorance” associated with the time-averaged location of a classical trajectory. I_C incorporates insights similar to Ref. [9] about orbit delocalization but is significantly easier to compute. We see that I_C correlates well with S_Q across a wide range of system dynamical behaviors and certainly does better than any attempt to correlate the entanglement with measures of chaos. We argue that the roots of this correlation may be traced to the fact that S_Q is equal to the sum of “diagonal” (I_Q) and “off-diagonal” (R_Q) matrix elements of the angular momentum operators computed with the Floquet eigenstates of the system, where I_C is the classical limit of I_Q , and R_Q has no classical analog. These operator averages resolve features at significantly smaller scale than naively expected from considering just the Floquet eigenstates alone.

Further, both the classical and quantum geometries reflect the symmetry properties of the underlying Hamiltonian. That is, both are organized around phase-space points of high symmetry [12]. Classically these are the stable and unstable classical periodic orbits. Since I_Q and R_Q also reflect the location of phase-space points of high symmetry, we obtain the observed correlations between classical and quantum behavior. We emphasize that our empirical results on the correlation between quantum and classical measures at small j make it necessarily true that the semiclassical perspective cannot apply; we develop a new explanation for the correlation we see, and we consider the possible applicability to higher j as well. However, the higher j regime is not the central focus of this paper.

In short, we show a strong correlation between classical dynamics and quantum entanglement. In contrast to the standard understanding we find that (a) this exists for the extreme quantum limit of a two-qubit system, where the correspondence principle cannot be evoked, (b) persists in the absence of chaos, and (c) is visible via single trajectory measures. We argue that this is (d) due to symmetry considerations alone. We also see other interesting features of the quantum entanglement dynamics not previously considered, specifically that these dynamics are demonstrably periodic or quasiperiodic as a function of number of kicks and κ . We discuss these issues in detail below, starting with a short introduction to the kicked top Hamiltonian.

II. BACKGROUND: THE KICKED TOP

The kicked top is a spin \vec{J} evolving under the Hamiltonian

$$H = \hbar \frac{\pi}{2\tau} \hat{J}_y + \hbar \frac{\kappa}{2j} \hat{J}_z^2 \sum_{n=-\infty}^{\infty} \delta(t - n\tau), \quad (1)$$

which describes the precession of \vec{J} around the y axis combined with a periodic shearing kick around the z axis. κ parametrizes the strength (nonlinearity) of the kick, while τ is the time between kicks. We pay attention to the system only immediately following each kick at times $T_n = n\tau$ and thus obtain a map (understood as the Poincaré map of the

Hamiltonian flow) and a discrete unit of time n defined by the number of kicks that have occurred.

Using this discrete time description, the quantum system is most conveniently studied via the Floquet operator [12]

$$\hat{U} = \exp\left(-i \frac{\kappa}{2j} \hat{J}_z^2\right) \exp\left(-i \frac{\pi}{2} \hat{J}_y\right). \quad (2)$$

If we expand an initial state $|\psi(0)\rangle$ in terms of eigenvalues $\{\xi_i\}$ and eigenvectors [13] $\{|\xi_i\rangle\}$ of \hat{U} , then we can write the state at time n as

$$|\psi(n)\rangle = \hat{U}^n |\psi(0)\rangle = \sum_i \langle \xi_i | \psi(0) \rangle^n |\xi_i\rangle. \quad (3)$$

As is standard, to allow for meaningful comparison with the classical limit, we restrict our attention to the behavior of states which are initially spin-coherent states, which are minimum uncertainty states for spin systems. These states are generated from the angular momentum eigenstate $|j, j\rangle$

$$|\psi(0)\rangle = |\theta, \phi\rangle = \hat{R}(\theta, \phi) |j, j\rangle. \quad (4)$$

Here the labels j indicate eigenvalues for \hat{J}^2 and \hat{J}_z , and the rotation \hat{R} is defined as

$$\hat{R}(\theta, \phi) = \exp[i\theta(\hat{J}_x \sin \phi - \hat{J}_y \cos \phi)], \quad (5)$$

where $\phi \in [-\pi, \pi)$, $\theta \in [0, \pi)$. These spin-coherent states are thus centered at some location on the sphere (θ, ϕ) , and these locations are the classical initial conditions against which their behavior is to be compared.

Following previous studies, we study the entanglement of the system by considering the situation where the spin J is composed of $2j$ spin-1/2 particles, or qubits, such that $\vec{J} = \sum_{i=1}^{2j} \vec{s}_i$ for individual spins \vec{s}_i . While several different types of entanglement measures can be considered, all of them have been shown to have essentially the same broad behavior. We focus on the measure most studied, the bipartite entanglement between any one of the qubits and the subsystem made up of the remaining $2j - 1$ qubits. This entanglement is quantified by computing the linear entropy

$$S = 1 - \text{Tr} \rho_1^2, \quad (6)$$

where ρ_1 denotes the density operator for any one of the qubits, obtained by taking the partial trace over the $2j - 1$ other qubits. Since the dynamics are restricted to the symmetric subspace of the total spin, the entropy can also be written as [6]

$$S = \frac{1}{2} \left[1 - \frac{1}{j^2} (\langle \hat{J}_x \rangle^2 + \langle \hat{J}_y \rangle^2 + \langle \hat{J}_z \rangle^2) \right]. \quad (7)$$

In the classical limit $j \rightarrow \infty$, the system is described by the point dynamics of an angular momentum vector which we describe by its coordinates (x, y, z) . Reference [12] gives the classical map F from time step n to $n + 1$ for this vector:

$$x_{n+1} = z_n \cos(\kappa x_n) + y_n \sin(\kappa x_n), \quad (8)$$

$$y_{n+1} = -z_n \sin(\kappa x_n) + y_n \cos(\kappa x_n), \quad (9)$$

$$z_{n+1} = -x_n. \quad (10)$$

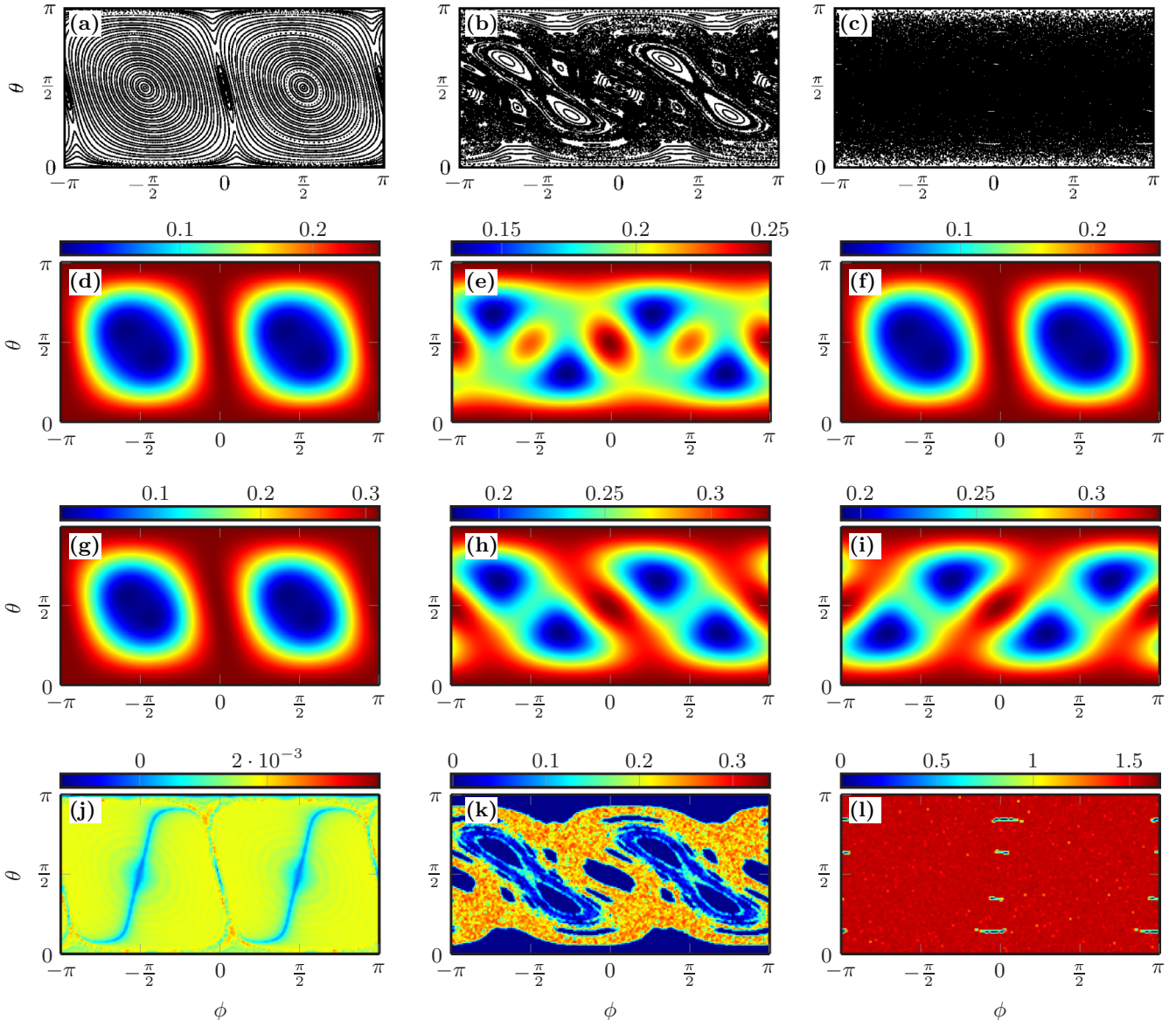


FIG. 1. (a) Classical Poincaré section for $\kappa = 0.5$. (b) Same but for $\kappa = 2.5$. (c) Same but for $\kappa = 2\pi + 0.5$. (d) Infinite-time averaged entanglement S_Q as a function of initial condition for two qubits for $\kappa = 0.5$. (e) Same but for $\kappa = 2.5$. (f) Same but for $\kappa = 2\pi + 0.5$. (g) Numerically computed (over 200 kicks) average entanglement S_Q as a function of initial condition for three qubits for $\kappa = 0.5$. (h) Same but for $\kappa = 2.5$. (i) Same but for $\kappa = 2\pi + 0.5$. (j) Finite time Lyapunov exponent (calculated over 2600 kicks) as a function of initial condition for $\kappa = 0.5$. (k) Same but for $\kappa = 2.5$. (l) Same but for $\kappa = 2\pi + 0.5$. Note that these are images of a sphere projected onto the plane, so that the left and right edges are connected and area is distorted. In particular, the polar regions around $\theta = 0$ and $\theta = \pi$ are the same size and shape as the regions around $(\theta, \phi) = (\pi/2, 0)$ and $(\pi/2, \pi)$. Also note the different scales for each plot.

Since total angular momentum is conserved [12], these dynamics occur on the surface of a sphere of unit radius, with the usual relation $(x, y, z) = (\sin \theta \cos \phi, \sin \theta \sin \phi, \cos \theta)$. The restriction to the surface of the sphere means that there are effectively two phase-space variables (θ, ϕ) . For low κ all initial conditions in the phase space show regular behavior. Around $\kappa \approx 1.0$, chaos emerges for certain initial conditions near unstable fixed points. The effect of increasing κ beyond this value is to increase both (a) the extent of phase space displaying chaotic behavior (the number of initial conditions displaying chaos) and (b) the degree of chaos—the rapidity with which initially infinitesimally close initial conditions separate in their trajectories. The behavior of a set of initial

conditions is shown for three different values of κ in the first row (a–c) of Fig. 1. We quantify the chaotic behavior in detail later when comparing the behavior with the quantum entanglement dynamics.

III. ENTANGLEMENT DYNAMICS OF THE TWO-QUBIT KICKED TOP

One of the advantages of working at small j is that for the smallest nontrivial quantum system ($j = 1$), we can carry out many calculations analytically that must be considered numerically even for $j = 3/2$. In particular, we find a closed-form solution for the entanglement $S(\theta, \phi, \kappa, n)$ as a function

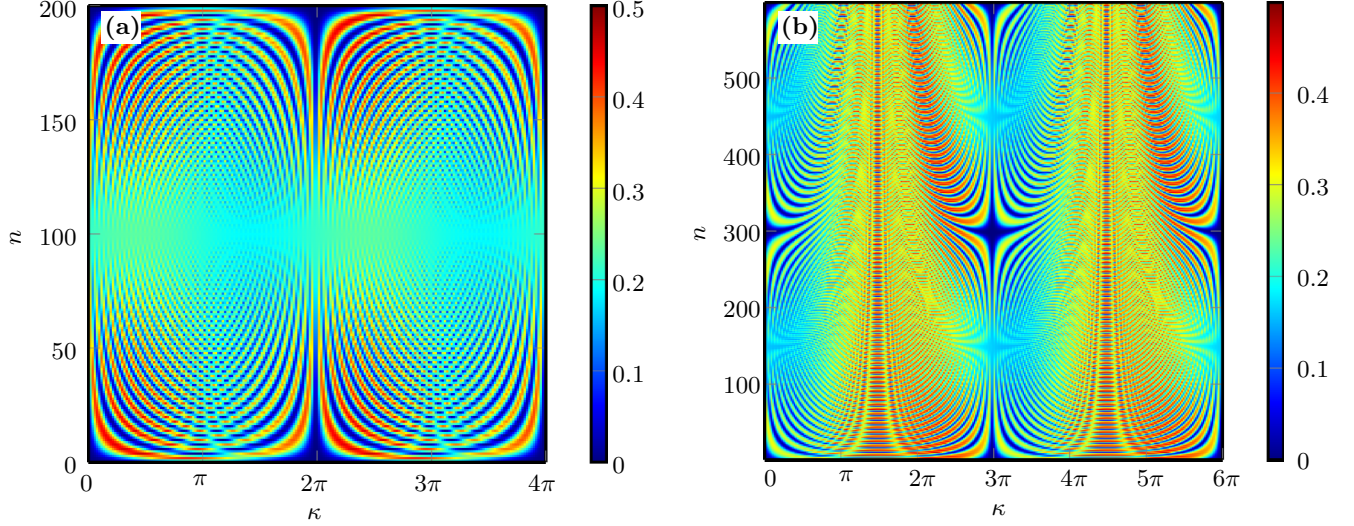


FIG. 2. (a) Entanglement entropy S plotted as a color (color coding shown in the bar on the right of both figures) for a two-qubit system ($j = 1$). It is plotted as a function of time n on the vertical axis and kick strength κ on the horizontal axis for an arbitrarily chosen initial condition $(\theta, \phi) = (1.2, 0.3)$. (b) The same, computed numerically for three qubits ($j = 3/2$) with initial condition $(2.5, 1.1)$. Note the (quasi-)periodicity in both κ and n , and the longer periods in both κ and n for three qubits compared to two qubits.

of initial position, kick strength, and time; this also allows an expression of its infinite-time average. If we examine the quantum “orbit” of the vector $\langle \hat{J} \rangle = (\langle \hat{J}_x \rangle, \langle \hat{J}_y \rangle, \langle \hat{J}_z \rangle)$, we can gain insight into the entropy as expressed in Eq. (7), since the length of this vector is the quantity of interest. The orbits are most easily understood by splitting them up into even and odd time steps, for kicking strength κ and initial condition $|\theta, \phi\rangle$:

$$\langle \hat{J}_x(n) \rangle = \begin{cases} (-1)^{n/2} \left[\sin \theta \cos \phi \cos\left(\frac{\kappa}{2} \frac{n}{2}\right) - \sin \theta \cos \theta \sin \phi \sin\left(\frac{\kappa}{2} \frac{n}{2}\right) \right] & n \text{ is even} \\ (-1)^{(n+1)/2} \left[\cos \theta \cos\left(\frac{\kappa}{2} \frac{n+1}{2}\right) + \cos \phi \sin \phi \sin^2 \theta \sin\left(\frac{\kappa}{2} \frac{n+1}{2}\right) \right] & n \text{ is odd} \end{cases} \quad (11)$$

$$\langle \hat{J}_y(n) \rangle = \begin{cases} \sin \theta \sin \phi & n \text{ is even} \\ \sin \theta \left(\sin \phi \cos \frac{\kappa}{2} - \cos \theta \cos \phi \sin \frac{\kappa}{2} \right) & n \text{ is odd} \end{cases} \quad (12)$$

$$\langle \hat{J}_z(n) \rangle = -\langle \hat{J}_x(n-1) \rangle. \quad (13)$$

The expression for $\langle \hat{J}_y(n) \rangle$ does not depend on n beyond its parity, which causes the orbits to lie in planes parallel to the xz plane in the shape of two deformed ellipses (at even n it is exactly an ellipse). When κ is an irrational fraction of π , the dynamics are quasiperiodic in n and this orbit is explored ergodically. If κ is a rational fraction of π , then the dynamics are periodic and a finite subset of the orbit is explored. This (quasi-)periodicity holds for higher values of j , as can be seen from the form of the Floquet operator [Eq. (2)] and the resulting eigenvalues. In general, the length of the period increases with increasing j , which is why this periodicity has not been observed in previous studies that focus on higher j .

These results allow an explicit evaluation of S , which we plot in Fig. 2 as a function of both κ and n for an arbitrary initial

condition $|\theta, \phi\rangle$; the (quasi-)periodicity is clearly visible in these “butterfly wing” plots. We can also take an infinite-time average $S_Q(\theta, \phi, \kappa) = \overline{S(\theta, \phi, n, \kappa)}$ that relies on the ergodic exploration of these orbits in the quasiperiodic case. We show S_Q for a selection of κ values in the second row (d–f) of Fig. 1. S_Q is also periodic in κ , and in fact the Floquet expansion shows that any finite- j system is also periodic in κ where this period increases with increasing j . For example, the Floquet eigenvalues of the two-qubit system are $\{e^{-i\kappa/2}, -ie^{-i\kappa/4}, ie^{-i\kappa/4}\}$, so the dynamics are unchanged if $\kappa \rightarrow \kappa + 8m\pi$ for any integer m . In particular, since there is no entanglement at all at $\kappa = 0$, there is also no entanglement for $\kappa = 8m\pi$. In fact, due to averaging effects, S_Q has period 2π in κ , which is confirmed by comparing the first and third columns of Fig. 1. We can also calculate the average entanglement for three qubits numerically, as shown in the third row (g–i) of Fig. 1. This calculation is necessarily a finite-time average, but it allows comparison with recent experiment [10] and shows that our observations are not unique to the two-qubit case.

As an alternative, for any number of qubits, S_Q can be written in terms of the Floquet eigenbasis (with $C_k = \langle \xi_k | \theta, \phi \rangle$) as

$$\begin{aligned} S_Q &= \frac{1}{2} - \frac{1}{2j^2} \sum_i \overline{[\langle \psi(n) | \hat{J}_i | \psi(n) \rangle]^2} \\ &= \frac{1}{2} - \frac{1}{2j^2} \sum_i \left[\sum_{k,l} (\xi_k^* \xi_l)^n C_k^* C_l \langle \xi_k | \hat{J}_i | \xi_l \rangle \right]^2 \\ &= \frac{1}{2} - \frac{1}{2j^2} \sum_{k,l,p,q} \sum_i C_k^* C_l C_p^* C_q \langle \xi_k | \hat{J}_i | \xi_l \rangle \langle \xi_p | \hat{J}_i | \xi_q \rangle \\ &\equiv \frac{1}{2} - \frac{1}{2j^2} \sum_{k,l,p,q} E(k,l,p,q) \\ &\quad \times \text{for } \{k,l,p,q : \xi_k^* \xi_l \xi_p^* \xi_q = 1\}, \end{aligned} \quad (14)$$

where the last line defines the $E(k, l, p, q)$ that we will discuss later. This essentially separates the “AC” components from the “DC” components (that is, the “AC” terms average to zero). Since the only time dependence is in the power of the product of the eigenvalues, which are all modulus 1 complex numbers, we have to satisfy the condition $\xi_k^* \xi_l \xi_p^* \xi_q = 1$ to find the DC components. However, since this is an *exact* condition, it is not trivial to use this equation for numerical work. The two-qubit case is the only one in which we can diagonalize \hat{U} entirely analytically, and hence the only case in which we can perform a straightforward computation of the “DC” results. However, this expansion yields theoretical insight, as we discuss in Sec. IV A.

IV. CLASSICAL CHAOS AND QUANTUM-CLASSICAL SIMILARITIES

To proceed further in comparing the quantum and classical initial condition dependence and behaviors, we start with quantifying the degree of chaos in the classical kicked top. To do this we use the (largest) Lyapunov exponent, which characterizes the time dependence of how two orbits initialized close together in phase space diverge. After choosing an initial point (θ, ϕ) , we evolve both the map and the tangent vector to the map, rescaling the tangent vector to a unit vector at each step. At each step the scale change in length is recorded and then averaged. Formally, the Lyapunov exponent is calculated as the average computed in the limit as $n \rightarrow \infty$. For an ergodic system, the infinite-time Lyapunov exponent is independent of initial condition. However for a generic classical Hamiltonian system Lyapunov exponents depend on the initial condition. Studies of this dependence, particularly as computed for finite-time Lyapunov exponents and their time-dependent convergence, have proved very useful in characterizing the phase-space geometry of dynamical instability in generic chaotic systems (see, for example, the discussion in Ref. [14]). In this system we see regular, mixed (regular and chaotic regions coexisting in phase space) and completely chaotic behavior as κ increases. We characterize these different behaviors by computing a finite time Lyapunov exponent (using $n = 2600$ and with transient behavior rejected by discarding the first 100 steps) and mapping the finite time Lyapunov exponent as a function of initial condition.

An example of how this finite time exponent is useful in ways the infinite time exponent may not be is visible in the figure at $\kappa = 0.5$. Here λ is not identically zero, even though the classical system is completely regular. All the deviations from zero are very small, and these can be shown to converge to 0 for $t \rightarrow \infty$. However, these “slow-to-converge” regions mark the invariant manifolds of the fixed points of the classical dynamics. The locations of these manifolds in fact determine the phase-space separation into stability “islands” and “chaotic sea” as κ increases. This underlines the idea (which we explore further below) that the phase space is organized around the fixed points of the map dynamics (simple periodic orbits of the flow).

With direct measures of both entanglement and chaos in hand, we now compare the entanglement of the quantum system to the chaos in the classical system as previously done in the literature. First, in comparing the first and second rows

of Fig. 1, it is immediately clear that the entanglement average has signatures of the classical orbits. That is, both classically and quantum mechanically, different initial conditions lead to very different behavior, and the boundaries between different behavior have approximately the same location and shape in both figures. This would seem initially to validate the previous consensus in the literature. However, the fact that this resemblance remains even in this extreme quantum limit means that all previous arguments—which relied on the semiclassical nature of the quantum system being studied—cannot hold. Further, this resemblance between the two different geometries exists without classical chaos, as evidenced by the similarities between graphs of the entanglement and the classical phase space [Figs. 1(d)–1(f) and 1(a)–1(c), respectively] at $\kappa = 0.5$. Finally, the plot of λ for the classical system at $\kappa = 2.5$ (third row) shows that although the shapes of regions around $(\theta, \phi) = (\frac{\pi}{2}, 0)$, $(\frac{\pi}{2}, \pi)$, $(0, 0)$, and $(\pi, 0)$ are similar to the shapes of regions in the entanglement plot, these regions have a low Lyapunov exponent but high entanglement. Both this anticorrelation and the similarity of region boundaries are particularly visible in Fig. 3, where S_Q and λ are plotted together along a line of initial conditions.

In general, we therefore see that both very high and very low levels of entanglement are correlated with different types of regular classical dynamics, but chaotic dynamics correspond to a level of entanglement about halfway between these extremes [15].

We also show a comparison at $\kappa = 0.5 + 2\pi$. Here the quantum entanglement geometry is clearly different from the classical phase-space geometry. This clear break in the similarities of the systems can be easily understood as arising from the fact that the quantum system is periodic in κ while classical phase space becomes increasingly chaotic as κ increases.

A. Classical and quantum “ignorance” (delocalization)

Since the similarities between the maps of initial-condition dependence of the entanglement and the classical Poincaré map cannot be explained by a direct connection between chaos and entanglement, we need to understand what other features of the dynamics renders the two so similar. In the following we argue that it is broad geometric features of the dynamics which provides this connection.

We start by considering that Eq. (14) can be rewritten as

$$S_Q = I_Q + R_Q, \quad (15)$$

$$\begin{aligned} I_Q &= \frac{1}{2} - \frac{1}{2j^2} \sum_i \overline{\langle \psi(t) | \hat{J}_i | \psi(t) \rangle}^2 \\ &= \frac{1}{2} - \frac{1}{2j^2} \sum_{k,q} E(k, k, q, q), \end{aligned} \quad (16)$$

$$\begin{aligned} R_Q &= -\frac{1}{2j^2} \sum_{k,l,p,q} \sum_i C_k^* C_l C_p^* C_q \langle \xi_k | \hat{J}_i | \xi_l \rangle \langle \xi_p | \hat{J}_i | \xi_q \rangle \\ &= -\frac{1}{2} \sum_{k,l,p,q} E(k, l, p, q) \\ &\quad \text{for } \{k, l, p, q : \xi_k^* \xi_l \xi_p^* \xi_q = 1, k \neq l \text{ or } p \neq q\} \end{aligned} \quad (17)$$

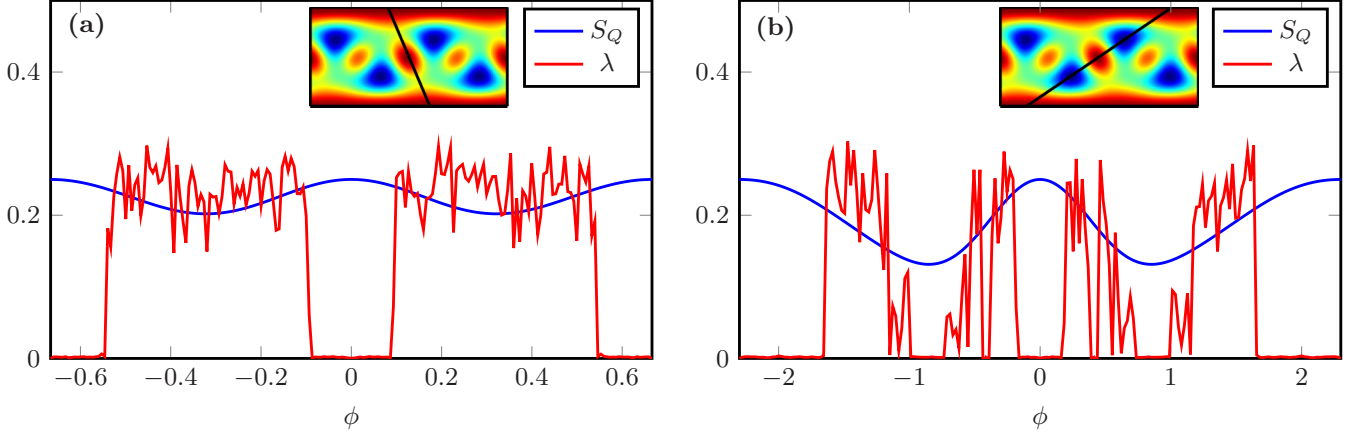


FIG. 3. (a) A slices of the plots of time-averaged entanglement S_Q and Lyapunov exponent λ at $\kappa = 2.5$. The slice taken is shown by the black line $\theta = (\pi/2)(\phi/\phi_0 + 1)$ superimposed on the plot of S_Q with $\phi_0 = -0.666018$. (b) Same except $\phi_0 = 2.29965$. Note the anticorrelation at the center and edges of both plots.

with the overbar indicating time averaging over an entire trajectory. I_Q is a global “ignorance” about the angular momentum for the trajectory-averaged distribution associated with a given initial condition. It is essentially a measure of the delocalization across the entire orbit, as the classical version below makes clear. The other “off-diagonal” remainder term is what we call R_Q and has no possible classical equivalent. These two measures are plotted in Fig. 4(d)–4(f) and Fig. 4(g)–4(i), respectively. We conjecture that if a correlation exists between S_Q and a classical quantity, it should be with classical limit of I_Q . This classical quantity can be written as

$$I_C = \frac{1}{2} - \frac{1}{2}[\overline{x(n)^2} + \overline{y(n)^2} + \overline{z(n)^2}], \quad (18)$$

which is plotted in Fig. 4(a)–4(c). Using this measure to compare with quantum dynamics incorporates the core idea of Ref. [9] that a classical orbit’s delocalization is relevant to the average entanglement of the corresponding quantum state. However, this does not evoke a correspondence principle assumption about the quantum and classical dynamics agreeing for any length of time. It also has the advantage of not needing the use of classical distributions, from which it is computationally exceedingly difficult to get converged results. Our conjecture relies on global averages correlating even when local in time behaviors are different. In fact, the plots of I_C show a remarkable similarity to the plots for S_Q that persists for $\kappa = 0.5, 2.5$ at least until the disconnect due to the quantum κ periodicity seen at $\kappa = 0.5 + 2\pi$.

Before proceeding further in exploring this possibly useful approach, we need to strengthen the claim that the visual resemblance between the plots of I_C and S_Q gives us more insight than the visual resemblance of the S_Q plots with the λ plots. To do so, we need to quantify a distance measure between the various figures.

B. Comparison of correlations

To make concrete the visual similarities and differences of the many plots in Fig. 1, we quantify the correlation between

any two quantities $f(\theta, \phi)$ and $g(\theta, \phi)$ as

$$D(f, g) = \ln \left[\frac{\text{Tr}(f)\text{Tr}(g)}{\text{Tr}(fg)} \right], \quad (19)$$

a generalized Kullback-Liebler distance [16]. Here Tr denotes the trace or double integral over the variables (θ, ϕ) . A small distance D implies good correlation, and vice versa. The behavior of this distance is shown in Fig. 5 for various quantities; note that we are plotting D on a logarithmic scale. This plot confirms that indeed $D(S_Q, \lambda)$ is large, that is, the entanglement and chaos are uncorrelated or weakly correlated. On the other hand, S_Q , I_Q , and I_C all show good correlation with one another, supporting our conjecture that if there is a connection between S_Q and a classical measure, it should be our ignorance or delocalization measure I_C . The extremely good correlation between I_Q and I_C for $\kappa < 1$ is due to the fact that the limits $j \rightarrow \infty$ and $\kappa \rightarrow 0$ are related, as can be seen from the Hamiltonian [Eq. (1)].

A source of disagreement (for larger κ values) between the classical and quantum measures is due to the κ -periodicity of the quantum dynamics as noted in Sec. III. Thus the quantum and classical geometries part company as the quantum system cycles through different behaviors in contrast to the increasing classical chaos. In general, this implies a distinct break in the quantum-classical connection after a specific $\kappa^{\max}(2j)$ depending on the number of qubits $2j$. Thus, when evaluating the correlation of various quantities we focus on $\kappa < \kappa^{\max}$.

We also see that although the entirely quantum terms comprising R_Q can be quite large compared to I_Q , this does not seem to significantly affect the correlation seen between S_Q and I_C . A clue to this may perhaps be found in the fact that although R_Q has no classical analog, its limiting behavior is determined by S_Q and I_Q . As $j \rightarrow \infty$ we must have $S_Q \rightarrow 0$ and $I_Q \rightarrow I_C$. Since $S_Q = I_Q + R_Q$, it therefore must be true that $R_Q \rightarrow -I_C$ in the classical limit. Thus, arguably any global reason for the correlation between S_Q and I_C could also apply to R_Q , although it is difficult to extend this further given that there is no classical analog for R_Q . Consequently, we focus below on S_C and I_C .

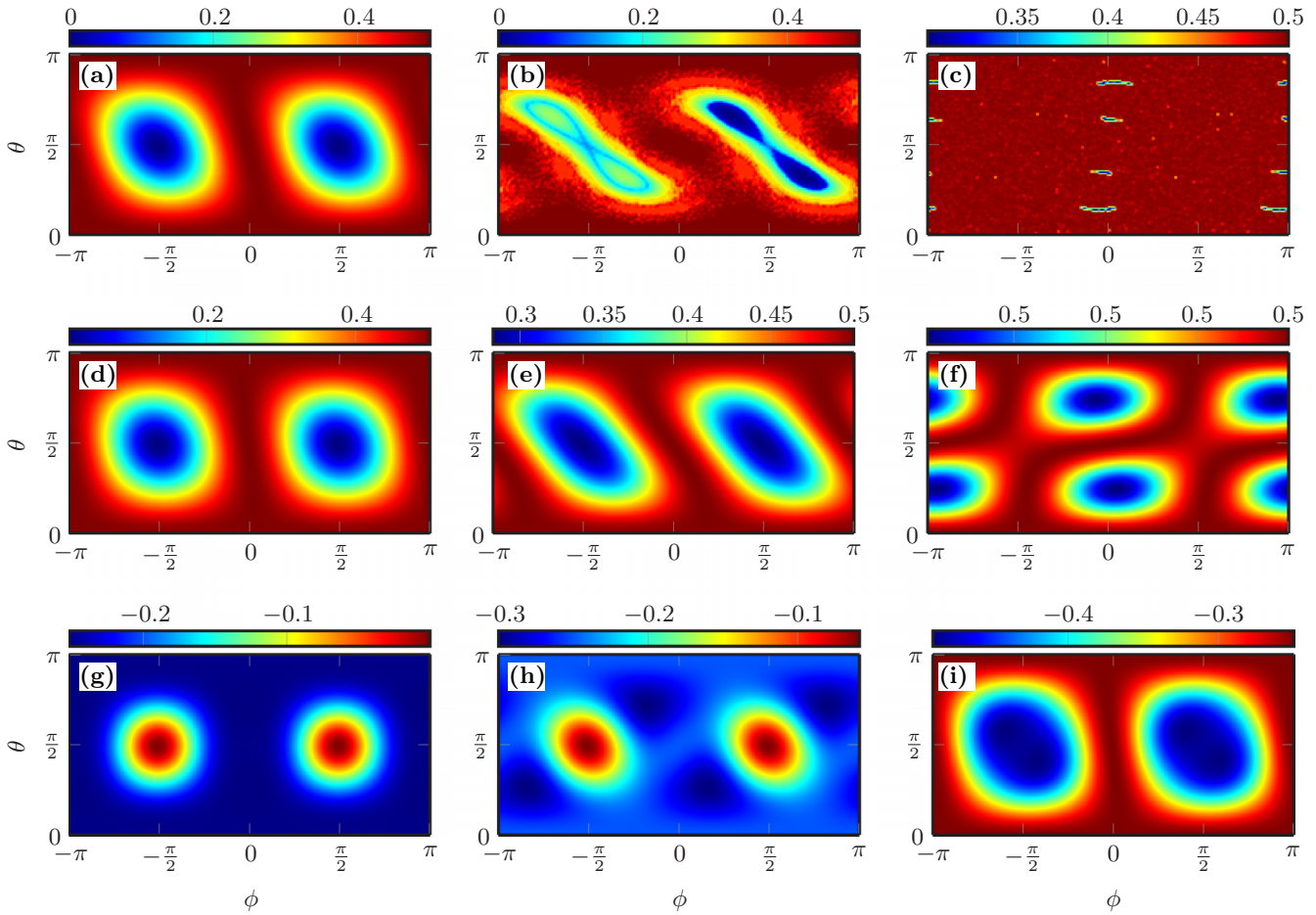


FIG. 4. (a) Ignorance measure I_C as a function of initial condition (θ, ϕ) for $\kappa = 0.5$. (b) Same but for $\kappa = 2.5$. (c) Same but for $\kappa = 2\pi + 0.5$. (d) Quantum ignorance measure I_Q as a function of initial condition for $\kappa = 0.5$. (e) Same but for $\kappa = 2.5$. (f) Same but for $\kappa = 2\pi + 0.5$. (g) Quantum remainder term R_Q as a function of initial condition for $\kappa = 0.5$. (h) Same but for $\kappa = 2.5$. (i) Same but for $\kappa = 2\pi + 0.5$. Note that although S_Q (Fig. 1) has κ period of 2π , I_Q and R_Q both have period 4π and so do not have the same behavior at $\kappa = 0.5$ and $\kappa = 0.5 + \pi$. Note the different scales for the different plots.

V. SHARED SYMMETRY

Some insights about these similarities that we have observed obtain from considering the symmetries associated with both the classical and quantum dynamics. Specifically, there are four classical symmetries [12] associated with the kicked

top dynamics. These arise from the fact that the classical map F is invariant under two nonstandard time reversals and rotation by π about the y axis, and F^2 is invariant under rotations by π about the x axis. Exact analogues of all four symmetries exist in the quantum map \hat{U} (see Ref. [12] for an extended discussion of these symmetries).

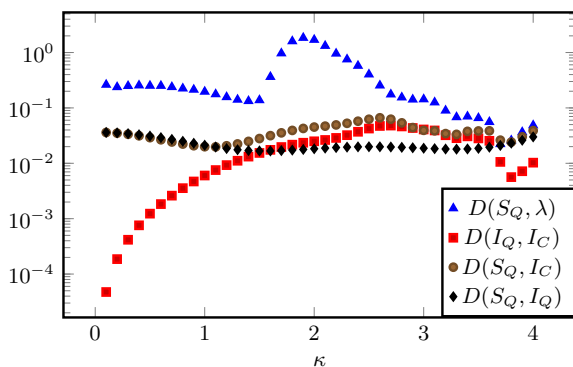


FIG. 5. Correlation distances D between entanglement and other measures. Values are only shown up to $\kappa = 4$, which is where the break due to quantum periodicity occurs for two qubits.

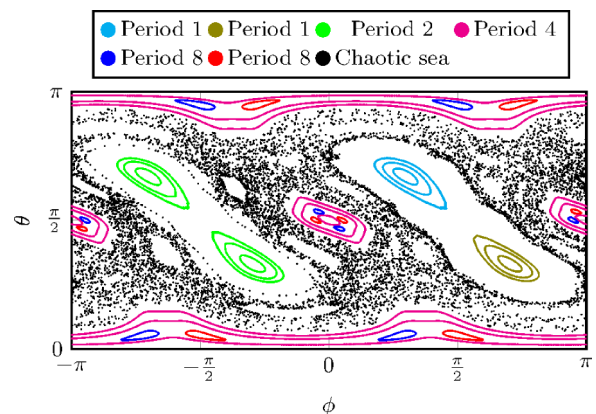


FIG. 6. Periodic orbits and surrounding stable islands for the classical system at $\kappa = 2.5$.

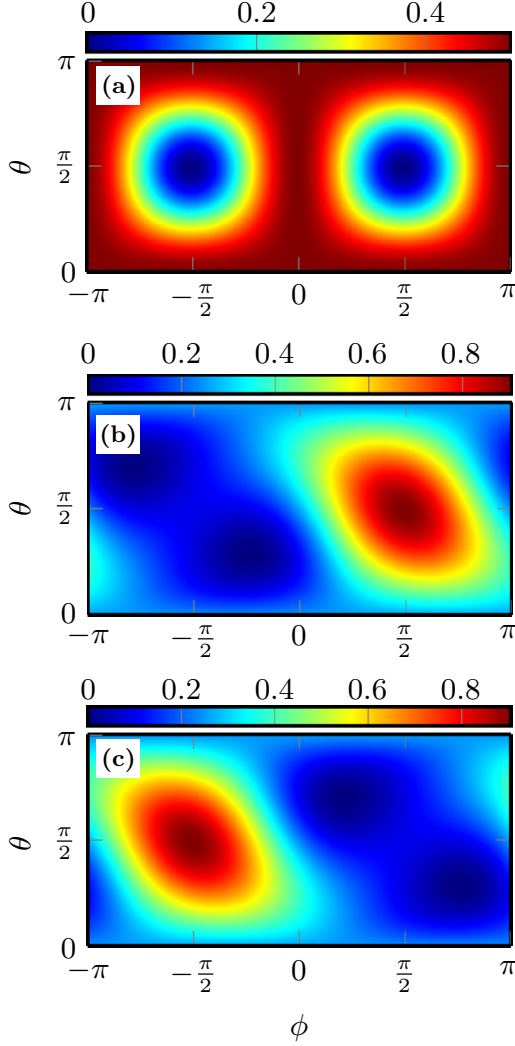


FIG. 7. The Husimi phase-space representation for the three eigenstates of the Floquet operator U .

The relevant aspect of these symmetries for our consideration here is to consider how different classical orbits organize. In Fig. 6 we plot the classical periodic orbits of different period, along with the associated islands of stability. The locations of these periodic orbits are determined by the classical symmetries. The actual locations of the periodic orbits change with κ , while the size of the stability islands around the periodic orbits also shrinks with increasing κ . Further, we expect that the Floquet eigenstates of \hat{U} naturally carry the same dynamical symmetries as the quantum map. While this is true (Fig. 7), what is striking about these states is that they seem far too large to resolve the smaller island structures seen in the classical phase space and the quantum entanglement figures.

We can unfold this apparent paradox by focusing attention on the actual operator averages we need to compute. As we see in Fig. 8, the dynamical symmetries of the quantum map (which are shared with the classical map) are also reflected in the plots of the various $E(k,l,p,q)$ that sum to I_Q (diagonal terms) and R_Q (“off-diagonal” terms). That is, the ability to resolve smaller-scale structures for the $E(k,l,p,q)$ is more

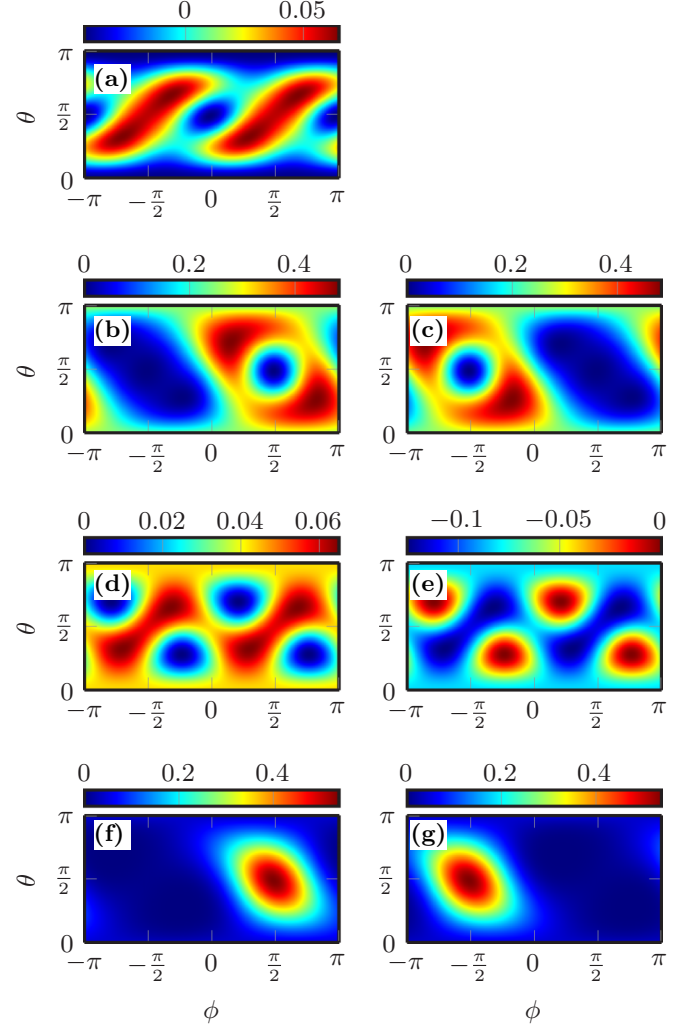


FIG. 8. Compact representation of the non-zero terms from the 81 different $E(k,l,p,q)$: we add the $E(k,l,p,q)$ that are identical or conjugates of one another. These are plotted as a function of θ , ϕ , at $\kappa = 2.5$. (a) The sum of $E(2,3,2,3) + E(3,2,3,2)$ (which are conjugates of each other, thus yielding a real result); (b) the sum $E(1,2,2,1) + E(2,1,1,2)$ (which are identical to each other); (c) the sum $E(1,3,3,1) + E(3,1,1,3)$ (which are identical to each other); (d) the sum $E(2,3,3,2) + E(3,2,2,3)$ (which are identical to each other); (e) the sum $E(2,2,3,3) + E(3,3,2,2)$ (which are identical to each other); (f) $E(2,2,2,2)$ (g) $E(3,3,3,3)$. Thus panels (b)–(e) sum to R_Q , and (a), (f), and (g) sum to I_Q . Note the different scales on each plot.

critical than the more spread-out shape of the eigenfunctions themselves. Comparing Fig. 8 of the various $E(k,l,p,q)$ with Fig. 6, and further comparing these plots with all the plots in Fig. 1 also makes clear that (a) both classical and quantum dynamics show signatures of the same symmetries and (b) quantities such as $E(k,l,p,q)$ and consequently S_Q as well as I_C reflect these phase-space symmetries. This leads to our argument that the long-observed correlation between measures of the classical and quantum systems arises from both kinds of phase space being organized around the symmetries of the dynamical system rather than any particular dynamical property such as the classical trajectories’ degree of chaos. Since

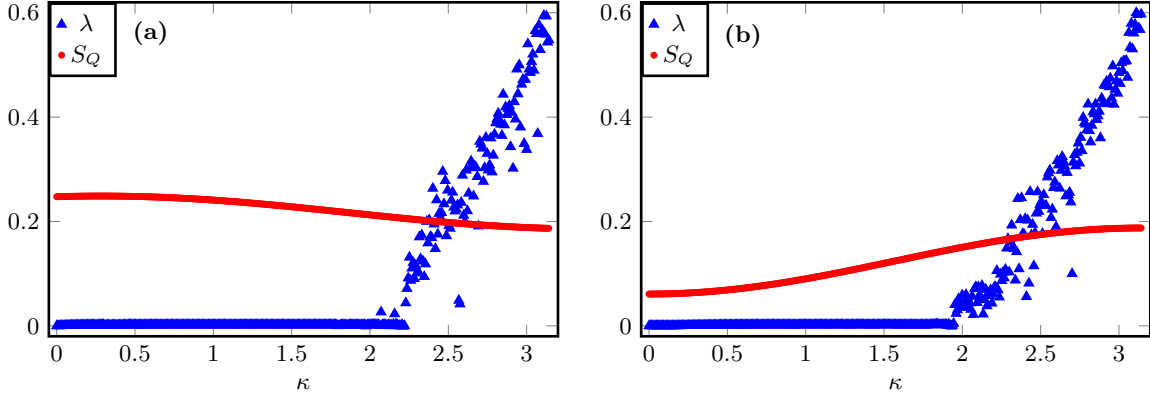


FIG. 9. (a) A plot of time-averaged entanglement S_Q and Lyapunov exponent λ as a function of κ with initial conditions, $(\theta, \phi) = (2.35, -0.1)$. (b) Same but with $(\theta, \phi) = (2.35, -\pi/2)$. These two figures demonstrate that although we can pick an initial condition so entanglement entropy and Lyapunov exponent appear correlated, this is not true in general.

classical stability islands and chaotic “seas” also organize around phase-space symmetries, this explains how a seeming association between chaos and entanglement can appear.

Focusing on the symmetries also allows us to separate the behaviors of those classical regular orbits that correspond to the highest quantum entanglement from those which correspond to the lowest entanglement—they are indeed orbits of very different symmetries. The organization of I_C around symmetry points is clear: points that are invariant under symmetries have $I_C = 0$, and those whose relationship to the symmetries causes them to move between a few small but distant areas on the sphere have maximal I_C . To relate the quantum entanglement to the symmetries, we can adapt the argument of Ref. [9] to relate each of these to the spread of the quantum state. Since total angular momentum is conserved, Eq. (7) can be rewritten in terms of the variances $\sigma_i = \sqrt{\langle J_i^2 \rangle - \langle J_i \rangle^2}$ in order to show that a state with higher spread is more entangled. Then, the initial states whose relationship to the symmetries is such that they get highly spread out over the sphere have a much higher average entanglement; intuitively, these are exactly the same initial conditions that classically end up with high values of I_C .

One effect that is not visible in the classical Poincaré map jumps out if the specific time period is noted for different periodic orbits (Fig. 6). For example, the largest islands are associated with a period-2 orbit for negative ϕ . This, however, looks very similar to the two period-1 orbits for positive ϕ . This explains the corresponding symmetry breaking in I_C [Fig. 4(a)–4(c)]. This symmetry breaking is not observed in any of the other plots of Fig. 1. However, this symmetry breaking was observed in plots of S_Q in a three-qubit experiment [10]. We may legitimately conjecture that this emerges in the experimental entanglement measures due to the dynamical difference of the symmetry breaking being enhanced by experimental noise or decoherence, although modeling that is beyond the scope of this paper.

VI. DISCUSSION

There are several points worth noting about the semiclassical and high κ limits of this analysis,

although both remain out of the scope of this paper.

We have remained focused on the observation that the most extremely quantum system shows shapes in the map of S_Q that resembles shapes in the classical phase space, albeit appearing as either correlation or anticorrelation between classical regularity and high or low quantum entanglement. Arguments previously advanced in the literature, particularly in the semiclassical limit, cannot apply. That is, *a priori* there cannot be a simple link between two-qubit dynamics and classical dynamics, even while the connection evidenced by the resolution of the S_Q plots invites an explanation. It seems clear, however, that the arguments we advance about symmetry and the $I_Q \rightarrow I_C$ connection should hold in the semiclassical case. This suggests that consideration of eigenstates which have increasingly sharper support in phase space at higher j values will not alter the overall relationship between quantum and classical dynamics.

Wang *et al.* [5] have argued that in the semiclassical regime, entanglement and chaos show similar dependence on increasing κ once the system has become fully chaotic ($\kappa > 3.5$). However, due to the small κ periodicity of the two-qubit quantum system, we do not expect any connection at all between the classical and quantum systems after $\kappa \approx 3$. Thus, we cannot examine the fully chaotic classical system in the context of our system.

Instead, we can explore the following. At higher κ values, the stability islands surrounding the periodic orbits become vanishingly small and the phase space is dominated by chaotic orbits. All chaotic orbits explore phase space in essentially similar ways, and in the absence of the periodic orbits that lead to either high or low entanglement, there should be little variation in the initial condition dependence of entanglement. However, in considering *only* the chaotic region, we have checked to see if at a given location and with varying κ there is any similarity between how λ changes compared with how S_Q changes. In Fig. 9 we show examples of our findings that there is essentially no correlation between the κ dependence of λ and S_Q : all initial conditions show essentially the same behavior for λ , and we can choose an initial condition to find essentially any behavior we like for S_Q . Some previous studies [2,5] have investigated the time dependence of the entanglement in the

semiclassical regime and found that quickly entangling initial conditions correspond with classically chaotic regions. Due to the very short period observed in the two-qubit case, the rate of entanglement is not a meaningful quantity in this study, and so we focus on the initial-condition dependence.

None of this would disagree with correspondence between quantum and classical behavior for the fully chaotic system in particular, as has been achieved using random-matrix theory [17].

We additionally note that both the symmetry observations and definitions of our ignorance measures are reliant on the spherical geometry of the phase space of the kicked top. It is unclear whether there exist analogues for other geometries, and thus whether such a connection between quantum entanglement and classical phase space maintains in other geometries. The restriction of this system to the symmetric subspace (via angular momentum conservation) is also essential our argument concerning the ignorance measures, since it gives the equivalence between entanglement and delocalization of the quantum state.

VII. CONCLUSION

We have demonstrated through numerical and analytical calculations consistent with recent experiments that entanglement, a quintessentially quantum phenomenon, is associated with the geometry of the classical phase space dynamics through the symmetries of the shared Hamiltonian. There is also a connection between the time-averaged entanglement of the quantum system and the ignorance (effectively delocalization) measures I_Q and I_C . We have seen this connection for two-qubit systems (the most quantum regime possible).

We also report that the entanglement dynamics are periodic or quasiperiodic in time depending on the nonlinearity parameter κ , as well as being a periodic function of κ . All of these results generalize to higher numbers of qubits.

There are several interesting directions in which this connection between entanglement and dynamical nonlinearity could be explored. The first is to understand better how the behavior changes as j increases. While we do discuss in general terms how increasing j works, a detailed analysis explicitly linking the very high j and the low j systems would be illuminating (albeit ambitious), particularly with regard to understanding the differences between finite-time and infinite-time averages of various quantities. A second approach is to understand the initial condition dependence of out-of-time-ordered-correlators [11] and determine whether this bridges some notions of quantum and classical information loss due to dynamics. It would also be worthwhile to understand the precise source of the differences in the quantum behavior of islands associated with different periods; as pointed out above, this classical difference remarkably seems visible in the three-qubit experiment [10] but not in the quantum calculations for either two-qubit or three-qubit systems. These should all help further clarify the relationship between entanglement and classical dynamics.

ACKNOWLEDGMENTS

We are grateful for funding from the Howard Hughes Medical Institute through Carleton College. We also acknowledge useful discussions with Pedram Roushan and Charles Neill, as well as Poul Jessen and helpful feedback from an anonymous referee.

-
- [1] K. Furuya, M. C. Nemes, and G. Q. Pellegrino, *Phys. Rev. Lett.* **80**, 5524 (1998).
 - [2] P. A. Miller and S. Sarkar, *Phys. Rev. E* **60**, 1542 (1999).
 - [3] A. Lakshminarayan, *Phys. Rev. E* **64**, 036207 (2001).
 - [4] S. Ghose and B. C. Sanders, *Phys. Rev. A* **70**, 062315 (2004).
 - [5] X. Wang, S. Ghose, B. C. Sanders, and B. Hu, *Phys. Rev. E* **70**, 016217 (2004).
 - [6] S. Ghose, R. Stock, P. Jessen, R. Lal, and A. Silberfarb, *Phys. Rev. A* **78**, 042318 (2008).
 - [7] S. R. Hudson, *Phys. Rev. E* **76**, 046211 (2007).
 - [8] S. Chaudury, A. Smith, B. E. Anderson, S. Ghose, and P. S. Jessen, *Nature (London)* **461**, 768 (2009).
 - [9] M. Lombardi and A. Matzkin, *Phys. Rev. E* **83**, 016207 (2011).
 - [10] C. Neill, P. Roushan, M. Fang, Y. Chen, M. Kolodrubetz, Z. Chen, A. Megrant, R. Barends, B. Campbell, B. Chiaro, A. Dunswoth, E. Jeffrey, J. Kelly, J. Mutus, P. J. J. O'Malley, C. Quintana, D. Sank, A. Vainsencher, J. Wenner, T. C. White, A. Polkovnikov, and J. M. Martinis, *Nat. Phys.* **12**, 1037 (2016).
 - [11] B. Swingle, G. Bentsen, M. Schleier-Smith, and P. Hayden, *Phys. Rev. A* **94**, 040302(R) (2016).
 - [12] F. Haake, *Quantum Signatures of Chaos* (Springer-Verlag, Berlin, 1991).
 - [13] Although strictly this notation assumes nondegenerate eigenvalues, this is neither necessarily true or needed, and we use it here only for convenience.
 - [14] A. Prasad and R. Ramaswamy, *Phys. Rev. E* **60**, 2761 (1999).
 - [15] Plots from previous studies [5] are consistent with this result, but their presentation via contour lines makes this particular relationship indistinguishable from strict correspondence between chaos and entanglement.
 - [16] A. K. Pattanayak, B. Sundaram, and B. D. Greenbaum, *Phys. Rev. Lett.* **90**, 014103 (2003).
 - [17] J. N. Bandyopadhyay and A. Lakshminarayan, *Phys. Rev. E* **69**, 016201 (2004).